

LA-UR- 87 - 2985

LA-UR--87-2985

DE88 000504

Los Alamos National Laboratory is operated by the University of California for the United States Department of Energy under contract W-7405-ENG-36

TITLE: REFUELING AND DENSITY CONTROL IN THE ZT-40M REVERSED FIELD PINCH

AUTHOR(S): G.A. Wurden, P.G. Weber, R.G. Watt, C.P. Munson,  
T.E. Cayton, and K. Buchl<sup>+</sup>.

SUBMITTED TO: International School of Plasma Physics Course & Workshop on  
"Physics of Mirrors, Reversed Field Pinches and Compact Tori"  
September 1-11, 1987, Varenna, Italy

<sup>+</sup>IPP, Garching, FRG

By acceptance of this article, the publisher recognizes that the U.S. Government retains a nonexclusive, royalty-free license to publish or reproduce the published form of this contribution, or to allow others to do so, for U.S. Government purposes

The Los Alamos National Laboratory requests that the publisher identify this article as work performed under the auspices of the U.S. Department of Energy

**Los Alamos** Los Alamos National Laboratory  
Los Alamos, New Mexico 87545

DISTRIBUTION OF THIS DOCUMENT IS UNLIMITED

MASTER

(XSL)

# Refueling and Density Control in the ZT-40M Reversed Field Pinch

G. A. Wurden, P. G. Weber, R. G. Watt, C. P. Munson,  
T. E. Cayton, and K. Büchl<sup>†</sup>  
presented by G. A. Wurden

Los Alamos National Laboratory  
Los Alamos, New Mexico, 87545 USA

<sup>†</sup> IPP, Garching, FRG

## Abstract

The effects of pellet injection and gas puff refueling have been studied in the ZT-40M Reversed Field Pinch. Multiple deuterium pellets ( $\leq 6 \times 10^{19}$  D atoms/pellet) with velocities ranging from 300–700 m/sec have been injected into plasmas with  $n_e \sim 1\text{--}5 \times 10^{19} \text{ m}^{-3}$ ,  $I_\phi \sim 100\text{--}250$  kA,  $T_e(0) \sim 150\text{--}300$  eV and discharge durations of  $\leq 20$  msec. Photographs and an array  $D_\alpha$  detectors show substantial deflection of the pellet trajectory in both the poloidal and toroidal planes, due to asymmetric ablation of the pellet by electrons streaming along field lines. To compensate for the poloidal deflection, the injector was moved up +14 cm off-axis, allowing the pellets to curve down to the midplane. In this fashion, central peaking of the pellet density deposition profile can be obtained. Both electron and ion temperatures fall in response to the density rise, such that  $\beta_\theta$  ( $\beta_\theta \equiv n_e(T_e(0) + T_i) / (\mathcal{D}_\theta(z))^2$ ) remains roughly constant. Energy confinement is momentarily degraded, and typically a decrease in  $F$  ( $F \equiv B_\phi(a) / (B_\phi)$ ) is seen as magnetic energy is converted to plasma energy when the pellet ablates. As a result of pellet injection at  $I_\phi = 150$  kA we observe  $T_e(0) \propto n_e^{-0.9 \pm 1}$ , while the helicity based resistivity  $\eta_k$  transiently varies as  $n_e^{-0.7 \pm 1}$ . While the achievement of center-peaked density profiles is possible with pellet injection, gas puffing at rates strong enough to show a 50% increase in  $n_e$  over a period of 10 msec ( $\sim 150$  torr-litres/sec) leads to hollow density profiles. The refueling requirements for parameters expected in the next generation RFPs (ZTH, RFX) can be extrapolated from these data using modified tokamak pellet ablation codes.

## I. Introduction

Since the operation of the first modern metal-walled RFP [1], and the use of active power crowbar circuits to sustain the RFP configuration [2,3], the control of density has become an issue. To zero<sup>th</sup> order, this is achieved through setting the

initial fill pressure, which defines the plasma density for times immediately after plasma breakdown. However, in all RFP's the density typically falls a factor of 5-10 from its peak initial value, usually leveling out, or slowly decaying in time for the remainder of the discharge. This phenomenon is referred to as "density pumpout", and is determined by a balance between particle confinement time and particle recycling to the vacuum vessel wall. A set of reference waveforms from a standard ZT-40M[4] discharge is shown in Figure 1, where pumpout is clearly visible in the interferometer density trace. The choice of material for the first wall

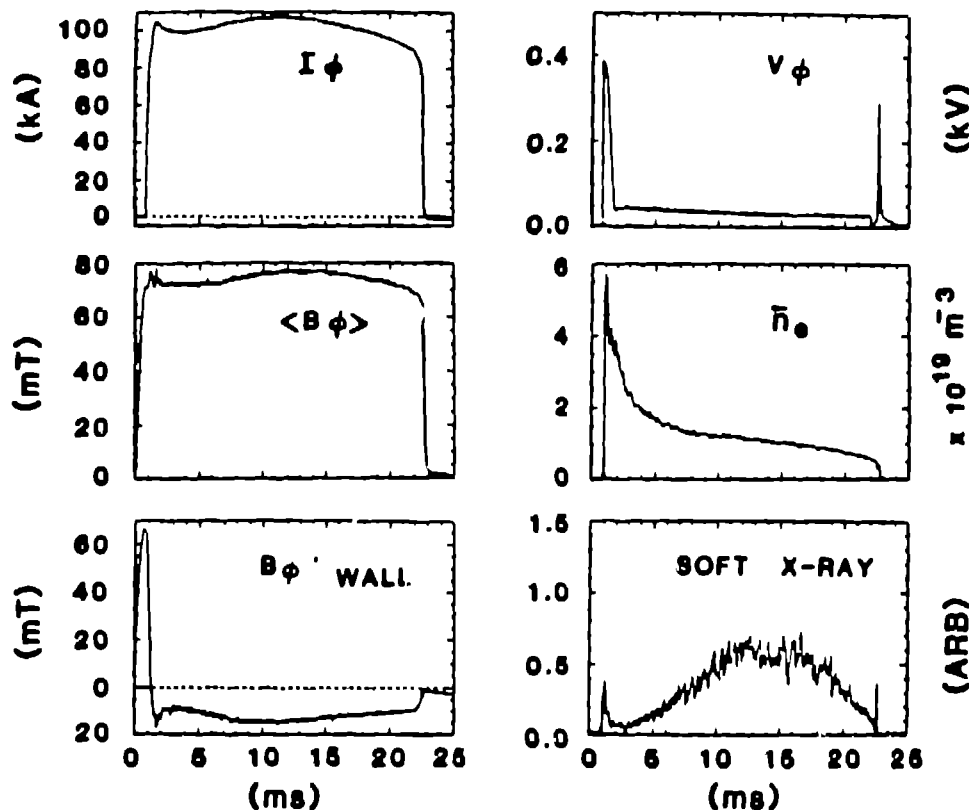


Figure 1: Typical flat-top ZT-40M waveforms, in the absence of any efforts at density control. Note the rapid pumpout of density initially, followed by a gradual decay. Circuits were fired at  $t=22$  msec to terminate the shot.

(for example, whether graphite or Inconel) will clearly have an important effect on recycling coefficients and hydrogen retention, and hence the density time behavior, but we take as a baseline case a dominantly metal-walled device, the most common situation in experiments to date.

We describe methods and techniques that have been found to be successful in giving the RFP operator an independent measure of control over the plasma density, and document the plasma response. Individual sections cover wall conditioning, gas puffing, and pellet injection, with principal emphasis on new results from pellet injection. In closing, expected refueling requirements for the next generation RFPs (ZTH and RFX) are discussed.

## II. Wall Conditioning

It is well known that the condition of the vacuum vessel wall affects plasma impurities, and particle recycling. Long term cleanup occurs after a vacuum opening, and the first few discharges of the day are different than those later on in a sequence of shots. Standard tokamak cleanup techniques, including glow discharge, pulsed discharge cleaning (PDC), and carbonization of the vessel wall, are used in RFP operations. Even after the wall is "clean", the wall has some memory of previous shots. Changes in the initial fill pressure often result in a hysteresis effect on the plasma density, taking several shots to stabilize. Likewise, it has been noted on ZT-40M, that heavy gas puffing results in subsequent shots being noticeably less reproducible with regard to density waveforms and equilibrium positioning.

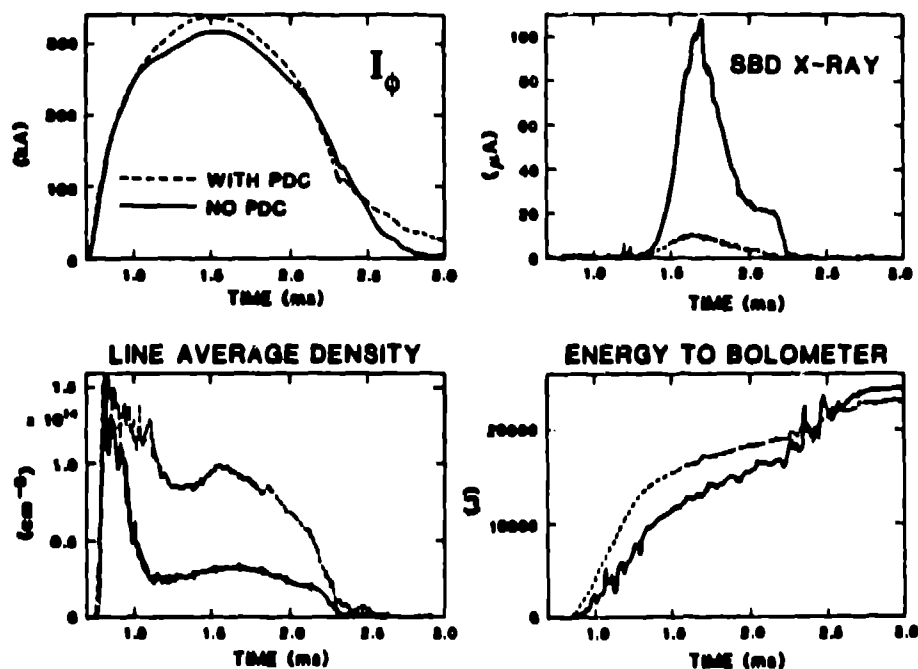


Figure 2: *Effects of Pulsed discharge conditioning on two consecutive round-top discharges. Electron density and current are higher, while soft x-ray emission, radiated power, and electron temperature are lower, at 1.2-2.2 ms.*

By incorporating pulsed discharge cleaning (at .5-1 Hz rep rate,  $\sim 30$  kA,  $\sim 1$  msec duration) for 45-90 seconds between normal RFP discharges in the computer controlled ZT-40M shot cycle, we have been able to "erase" the wall's memory of the previous high current RFP pulse. An added benefit was an increased plasma density (at the same initial fill pressure) for up to  $\sim 5$  msec into the plasma discharge. Figure 2 compares shots before and after the application of PDC immediately prior to the main discharge. PDC results in lower absolute levels of oxygen impurity, a higher final current for the same capacitor bank settings, a reduced resistivity anomaly factor, and improved electron energy confinement time, even though the on-axis electron temperature is substantially lower than without PDC[4]. By running the PDC at different fill pressures, varying amounts of hydro-

gen can be "preloaded" into the Inconel vessel wall, which consequently changes the plasma density during the shot as it is "unloaded" into the discharge by plasma bombardment. Alternatively, "sacrificial" high pressure shots can be fired before the "good RFP" shot, to achieve a similar wall loading effect[5].

In contrast to a metal wall, a full graphite wall has significantly different hydrogen retention properties[6]. On a shot to shot basis, OHTE with full graphite armor[7] experienced little or no control over the actual plasma density. The application of PDC to a relatively small percentage coverage of room temperature graphite in ZT-40M can excessively load it with hydrogen. However, our experience with limited armor coverage indicates that glow discharge can unload the hydrogen from the graphite. Operation after deposition of  $\sim 40$  monolayers of carbon (via glow discharge in a  $D_2$  plasma with a few percent methane), so-called "carbonization", proved to be intermediate between metal wall and 100% graphite in its effect on density[8]. Sustained elevated wall temperatures and careful shot sequences will be required in the next generation graphite-walled RFP's to control the density.

### III. Gas Puffing

Gas puffing experiments have been performed on the longer pulse length RFP's (ZT-40M and HBTX) for a number of years. Even with fast acting piezoelectric valves, flow rise times at the vacuum vessel liner are several milliseconds, as compared to a discharge length of  $\sim 10-20$  msec. Consequently, active feedback control of density (as is typically done in tokamaks), is not practical. Additionally, because of the relatively short particle confinement times ( $\tau_p \sim 1$  msec), large gas flows of order 100 torr-l/sec are required for significant plasma density response. To get reproducible results, the gas puff refueling should dominate the walls as a fueling source—no easy feat in relatively small, short pulse length devices.

In ZT-40M, four fast gas puff valves, one in each machine quadrant, have been used to raise the line average density by up to a factor of two in the later half of the discharge, with total flow rates of  $\sim 200$  torr-l/sec. Three 130 kA shots, the first with no gas puffing, are shown in Figure 3. A delay of 1-2 msec between the electrical pulse to the valves, and the actual plasma response, is noticeable. The density rise correlates well with amplitude of the local  $D_a$  detector near the puff valve(s). It has been postulated that low density (high  $I/N$ ) can cause instabilities leading to current termination[9], but it is clear that too high an edge density brought about by excessive gas puffing (with correspondingly low electron temperature) is equally dangerous, leading to a loss of field reversal, and then termination. Sometimes when this happens a low current, low field, high  $q$  tokamak discharge persists for 1-2 milliseconds, after the loss of reversal.

The neutral source remains highly localized toroidally, as measured with local and remote  $D_a$  detectors and photos. When the valves are shut off, the rising density flattens out, before the shot termination. Even with PDC between shots, shot-to-shot reproducibility is imperfect with gas puffing. This sometimes correlates

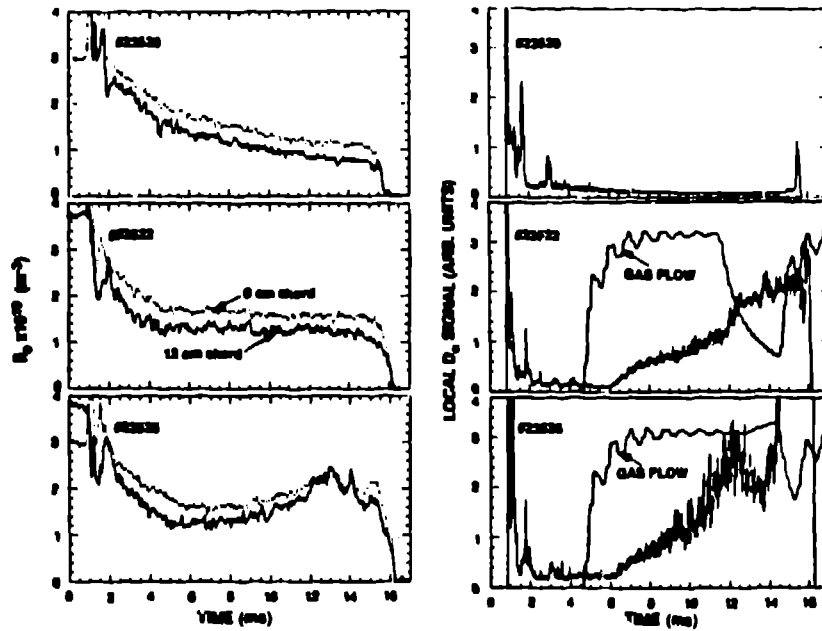


Figure 3: Line average electron density response to varying amounts of gas puffing. Center chord denoted by the light line, edge chord by heavy line. The density profile becomes edge peaked as a result of the puffing, late in the discharge. Flow sensor at one gas puff valve represents puff timing, while local  $D_\alpha$  monitor in that toroidal section shows the fueling rate at that toroidal location. Maximum rate per valve is 60 torr-l/sec, with three valves in use here.

with equilibrium positioning or variations in gas delivery by the valves (monitored at the valve), but is not fully understood. As timescales become longer in larger machines, distributed gas puffing should become more effective, but maintaining a center-peaked electron density profile with gas puffing may be challenging.

It has been observed in a number of machines[10,11,12], that the poloidal electron beta,  $\beta_\theta$ , is highest towards the low end of the I/N operating window. It is also the case in flattop discharges without explicit density control, that the electron energy content (as measured by  $n_e(0)T_e(0)$  or  $\bar{n}_e T_e(0)$ ) is usually higher earlier in time, compared to later as the density decays. While this could be an I/N effect, it could also be due to increasing impurities or progressively worse field errors as the magnetic fields penetrate into the conducting shell. The field error possibility is eliminated (at least temporarily) in gas puff discharges, where the I/N can be lowered up to a factor of two, while holding the toroidal current fixed. Figure 4 compares 180 kA discharges, with and without gas puffing, using central Thomson scattering for  $T_e$  and line average density  $\bar{n}_e$ . The electron beta appears to be marginally higher with puffing, subject of course to unmeasured profile changes and errors. This is not to say that the true poloidal beta is necessarily changed, since an interpretation of a beta dependence on I/N is subject to changes in ratio  $T_i/T_e$ , usually a poorly measured quantity in RFPs to-date. This is discussed in the other ZT-40M paper[13] presented at this School, where evidence points to a  $T_i/T_e$  ratio dependence on the parameters I/N and  $\theta$ .

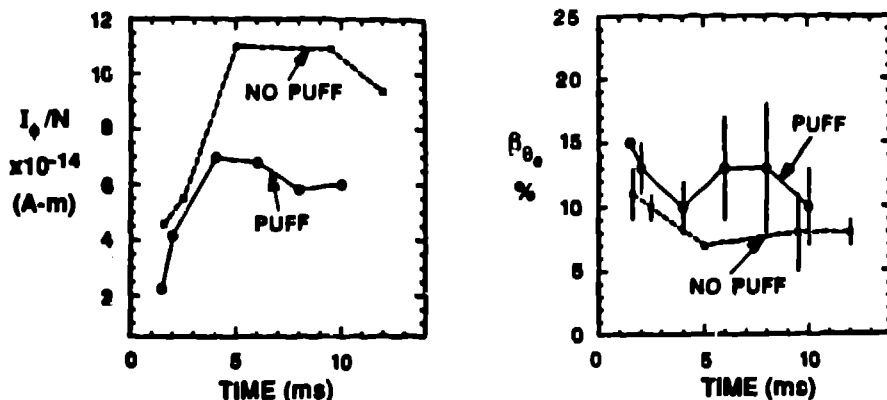


Figure 4: Decrease of electron poloidal beta in time is suppressed with gas puffing.

## IV. Pellet Injection

A natural choice to obtain peaked density profiles as the neutral particle penetration depth decreases in hotter and denser plasmas, is to use pellet injection to place the fueling source near the center of the plasma column. While this has become routine in tokamak plasmas[14], it has only recently been attempted in RFP plasmas[15,16,17]. Tokamak pellet ablation modeling applied to RFP parameters underestimates the size and velocity requirements, and surprises occur in the pellet trajectory. The discussion begins with on-axis injection results and photos, continues with theoretical modeling, off-axis injection for density peaking, details of the plasma response, and ends with projections for ZTH and RFX requirements.

### a) Initial Experiment: Midplane Launch

By modifying the Alcator C pellet injector for use on ZT-40M[18,19], hydrogen and deuterium pellets have been launched into the ZT-40M RFP. Initial results showed primarily edge deposition, as the pellet trajectory closest approach to the axis was typically  $\sim 7$  cm, when the pellet was small enough or slow enough for complete ablation[16]. The unexpected problem arose from large poloidal deflection of slow pellets (300-500 m/sec), or overpenetration at low currents of relatively straight trajectory fast pellets (500-700 m/sec). A 6-channel fanned  $D_\alpha$  array[20] first indicated the poloidal deflection, under the assumption of constant pellet speed in the plasma. Typical density responses are shown in Figure 5, where central (0 cm) and "edge" (+12.4 cm) FIR density traces during multiple pellet injection show edge peaked deposition at  $I_p = 120$  kA, and only moderately peaked density at 180 kA. The time response of the FIR interferometer is  $\sim 30$  kHz, and it does not routinely track the fast initial plasma breakdown startup spike. The four barrels of the injector have a 1 cm vertical separation, and we denote them as #1 through #4, from top to bottom. ZT-40M is usually operated in deuterium, and after first learning to run the injector with hydrogen (which is easier), we now routinely

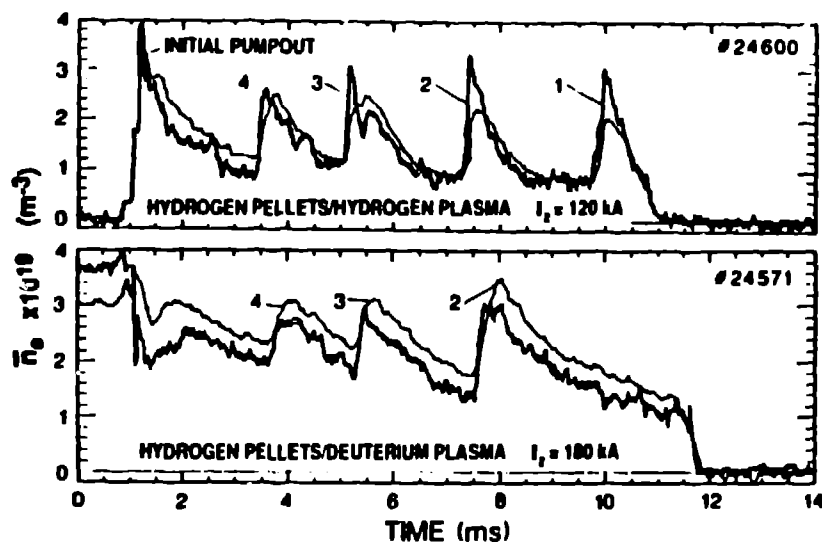


Figure 5: Interferometer density response to multiple pellets, midplane launch. At  $I_p = 120$  kA, the edge chord rises higher, and more quickly than the 0 cm central chord (dark line), while at higher current, pellet deposition is more central.

use deuterium pellets, because the 100l liquid helium dewar lasts longer (about 8 hours).

Time integrated top view photos show ablation tracks which curve in the local electron drift direction toroidally. In the photo Figure 6, two curving pellet tracks are visible. The dark hole in the center of the photo is the bottom central port, while the lines looking like ripples are the bellows convolutions. The two dark bands are two split poloidal graphite ring limiters, of which there are a total of eight around the torus. At first glance, the radial penetration (just past the center) of the pellets appears quite satisfactory, but in fact the pellets almost hit the bottom of the torus due to a strong poloidal deflection downwards. Reversing the direction of  $I_p$  reverses the toroidal deflection, while reversing  $B_p$  changes the direction of the poloidal deflection. Only 1/3 to 1/2 of the pellet inventory is observed as plasma density, consistent with ongoing plasma losses during the ablation process. This is substantially better than the factor of 20 loss during gas puffing over 10 msec timescales, while both results are consistent with ionized particles being lost to the wall, and not returning on timescales of the discharge.

## b) Ablation Modeling

A number of models have been developed over the years to describe the ablation of a cold dense hydrogen ice pellet in a plasma. These range from a simple neutral gas shielding cloud[21], which assumes that energy is carried to the pellet by a monoenergetic beam of electrons, to multi-electron group self-limiting models[22,23] where a more realistic incident energy flux is used, and magnetic shielding of the pellet by ionized ablatant is included. Self-limiting refers to the use of energy conservation in flux surfaces on pellet transit timescales, so that the population of

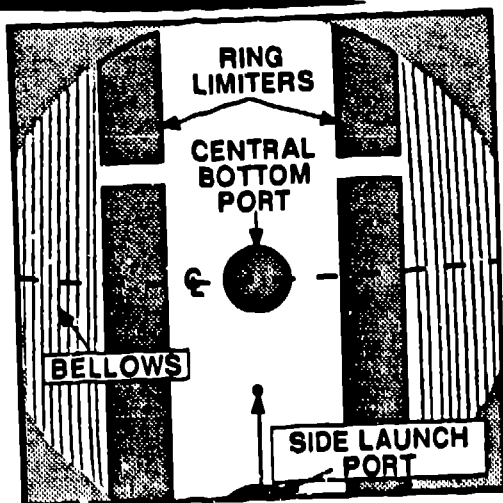
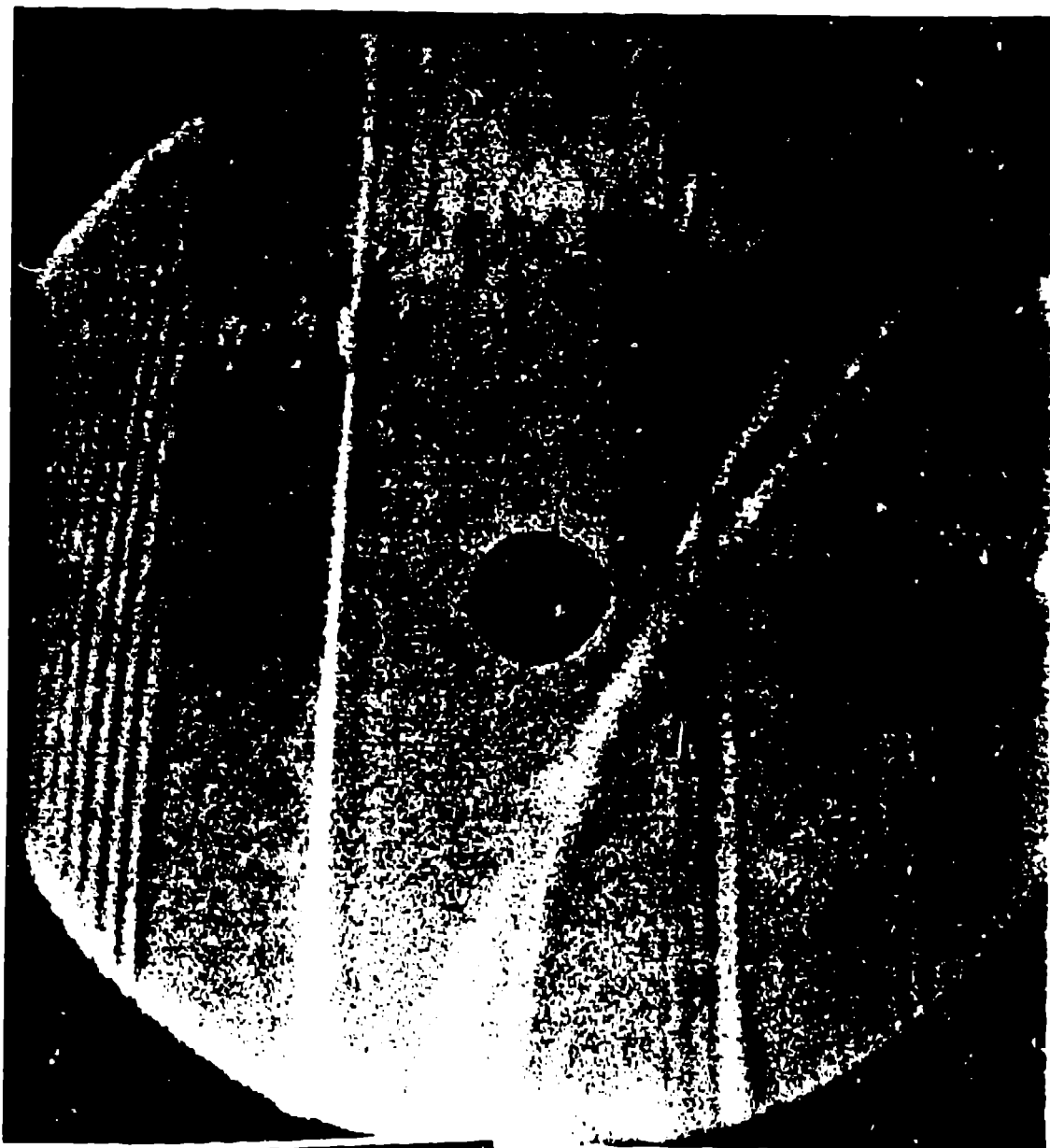


Figure 6: Top photo showing two pellets launched along the major radius from the horizontal midplane at a 10 cm diameter pump port. The pellets deflect toroidally to the right, due to differential ablation by electrons along field lines creating a "rocket" effect.

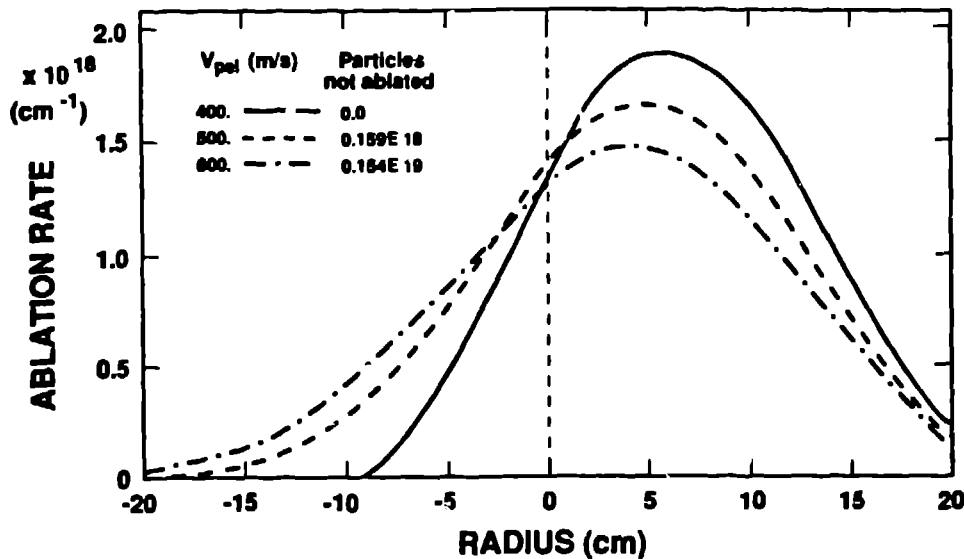


Figure 7: Multi-electron group Milora-Foster model prediction of deuterium pellet ablation rate for three different pellet velocities, using typical ZT-40M plasma parameters.  $T_e(0) = 250 \text{ eV}$ ,  $n_e(0) = 3 \times 10^{13} \text{ cm}^{-3}$ , parabolic profiles, but with edge temperature and density of 30 eV and  $5 \times 10^{12} \text{ cm}^{-3}$ . Thermal ablation only. The pellet radius is  $r_{\text{pel}} = 0.5 \text{ mm}$ , and has a content of  $3.09 \times 10^{19}$  atoms.

electrons responsible the ablation may become depleted as the pellet ablates. Using assumed parabolic density and temperature profiles, with self-limiting turned off, the Milora-Foster code predicts ablation rates shown in Figure 7. For the case of a tokamak, it is usually assumed that, on the timescale of the pellet ablation, the Ohmic or Beam input energy is small compared to that already in the plasma—hence the self-limiting model. In the absence of an accurate energy input model for an RFP, where ohmic input and pellet ablation timescales are nearly identical, we find better agreement with the experiment to leave self-limiting off—the effect being to ablate into a “fixed” plasma profile. More careful examination of the data shows that this is not truly the case, but that additional ablation (beyond thermal) is required in the edge region.

Slideaway electron populations have been loosely documented in TPE-1RM, HBTX-1B, and ZT-40M via SiLi soft x-ray spectra[24,25,26]. The presence Indeed a tail population at the 1% concentration, with 10x the local  $T_e$  has been directly measured in the extreme edge of ZT-40M[27]. The presence of a directed electron flux along magnetic field lines has a dramatic effect on both the pellet ablation rate, and the subsequent pellet trajectory due to differential ablation.

To explain the pellet trajectories, we have employed a phenomenological model of reaction thrust exerted on pellets that ablate non-uniformly over their surfaces[28]. An unbalanced electron flux flowing anti-parallel and parallel to the magnetic field lines in a current-carrying plasma results in differing ablation rate from one side of the pellet to the other. This model has successfully simulated the qualitative and quantitative features of the observed pellet trajectories, and also predicts a dependence of the deflections on the parameter  $I_\phi/N$  of the target plasma.

One may readily show that a single-component, drifting Maxwellian electron distribution with drift parameter  $\xi = 0.1$  yields an energy flux that is 40% larger on the electron drift side than on the ion drift side. If a 2-3% electron tail population at  $4 \times v_{thermal}$  is present, the asymmetry exceeds 2:1, and the total power delivered to the pellet is 60% higher than that from a simple thermal plasma alone. Figure 8 shows calculated top and side views of pellet trajectories for different asymmetry factors, and three types of launch positions—horizontal midplane, high side, and an upward angle or “ski jump deflection”. Orientation of  $B_\phi$  and  $I_\phi$  on axis is clockwise viewed from above, while pellets enter from the right. This case assumes pellets with  $v_{pel} = 500 \text{ m/sec}$ ,  $r_{pel} = 0.7 \text{ mm}$ , are tossed into a representative force

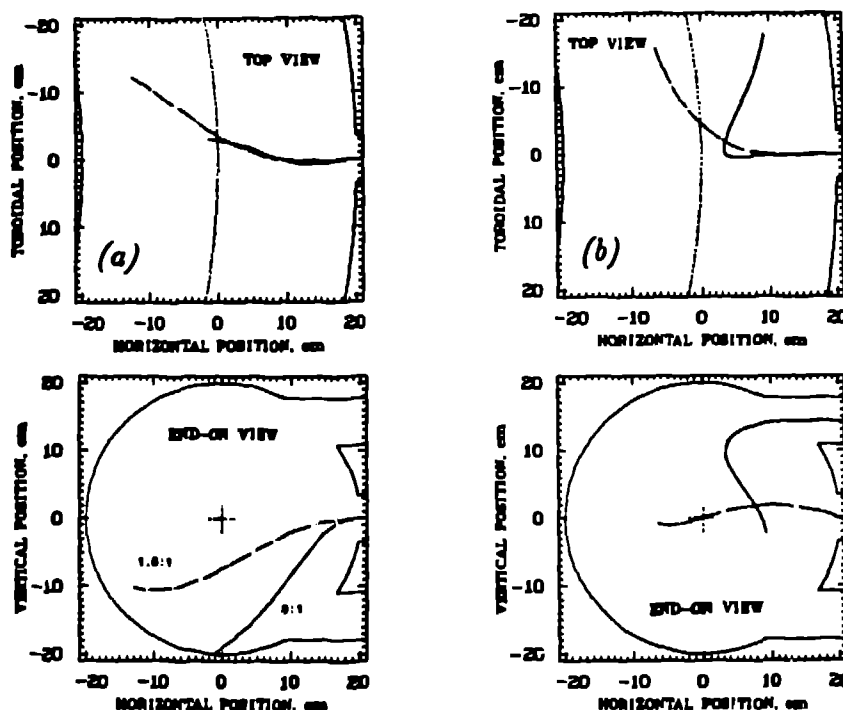


Figure 8: Simulated top and side views of pellet trajectories. (a) Midplane launch, two different asymmetry factors, 1.5:1 and 3:1. (b) Comparison of expected high side launch trajectory with midplane “ski jump” upwards initial trajectory of  $20^\circ$ .

free RFP magnetic configuration. In this simple approximation, the ablation rate, asymmetry factor, and the effective ejection speed[21]  $u_0 = 2.5 \times 10^8 \text{ cm/s}$  of the ablatant are all held constant in time and space. In (a), the strongly deflected pellet has  $\dot{M}_1 + \dot{M}_2 = 0.43 \text{ g/s}$ ,  $\dot{M}_1 : \dot{M}_2 :: 3 : 1$ , while the other has  $\dot{M}_1 + \dot{M}_2 = 0.25 \text{ g/s}$ , with only a 1.5:1 asymmetry ratio.  $\dot{M}_1$  and  $\dot{M}_2$  denote the rates of ablatant ejection parallel and anti-parallel to the local magnetic field. The deflections are always in the electron drift direction. Case (b) shows that the core of the plasma might be accessible by “dropping” the pellets from a high side launch, or “pitching” them in at an upward angle from the midplane position. We also expect from this model, that reducing the drift parameter, or removing a possible fast electron tail, will result in a reduction in the pellet deflection. In this fashion, the first pellet fired into the plasma may act as a shield for subsequent pellets, depending on the

timing between sequential pellets and timescales for regeneration of fast electrons.

### c) Off-axis Launch

In order to obtain on-axis peaking of the plasma density profile during the pellet ablation, it was clear from the experiment that we needed to reorient the gun, or suppress the pellet deflections in the plasma. To better aim the pellets for the center, as the result of predictions of the above described asymmetric ablation code modelling, we moved the gun to a high side launch position, +14.3 cm above the axis, in a 5 cm diameter horizontal side port. A single large pellet is shown in Figure 9 executing a 90° turn when viewed from above, while the resulting density trace (Figure 9(b)) has a long central chord density decay time, compared to the rapid edge density decay. The curvature is consistent with the electron drift direction in the plasma core. In a similar shot, shown in Figure 10, the tangential view is available as the pellet is deflected downwards to the axis.

Unfortunately, the port is somewhat higher than optimal, resulting in the pellets coming in almost tangent to the plasma magnetic field reversal layer. Some pellets are observed to stop in the plasma without deviation. Others are actually seen to deflect upwards (very unusual), and at the same time in the opposite direction toroidally as normally observed. This indicates that such a pellet spent most of its life outside of the reversal layer, where electron flow is in the opposite toroidal direction. The upwards deflection can only be accounted for by the effects of ablation into a steep plasma profile gradient, as the poloidal electron flow is thought to be unidirectional. By tilting the injector downwards 6.5° at the high side port, the reversal layer could be avoided more often, and the pellet has a longer possible path length through the plasma. This resulted in the observed frequency of peaked density deposition profiles going from only ~ 10% of the time with the old midplane position, to nearly 50% for this new launch technique.

### d) Midplane "Ski Jump" Launch

More recently, the injector was repositioned back to the horizontal midplane, but with the addition of a sloping 8° deflector plate, to act as a pellet "ski jump", with the intent of launching pellets upwards by elastically reflecting off of a room temperature stainless steel surface. At 400 m/sec, the pellets should remain intact, and bounce upwards at +16° near the plasma edge. The lower two barrels (out of four in the gun) should shoot pellets onto the plate, while the upper two should miss it most of the time. Up to 70% of the pellets show central density peaking in this configuration for 150 kA shots. Usually, the two chord FIR shows that the initial density profile is maintained throughout the ablation process, in sharp contrast to the flat or hollow profiles reported for horizontal launching[16].

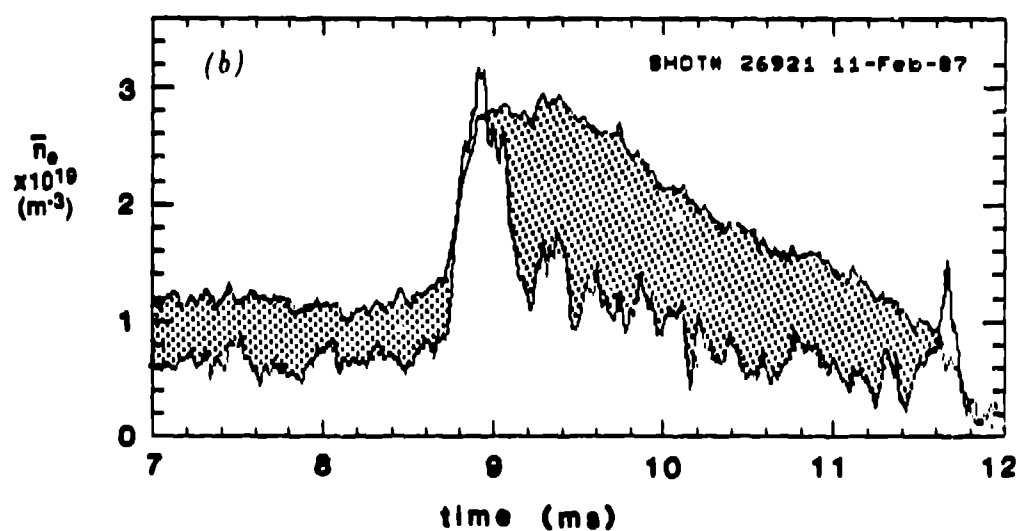
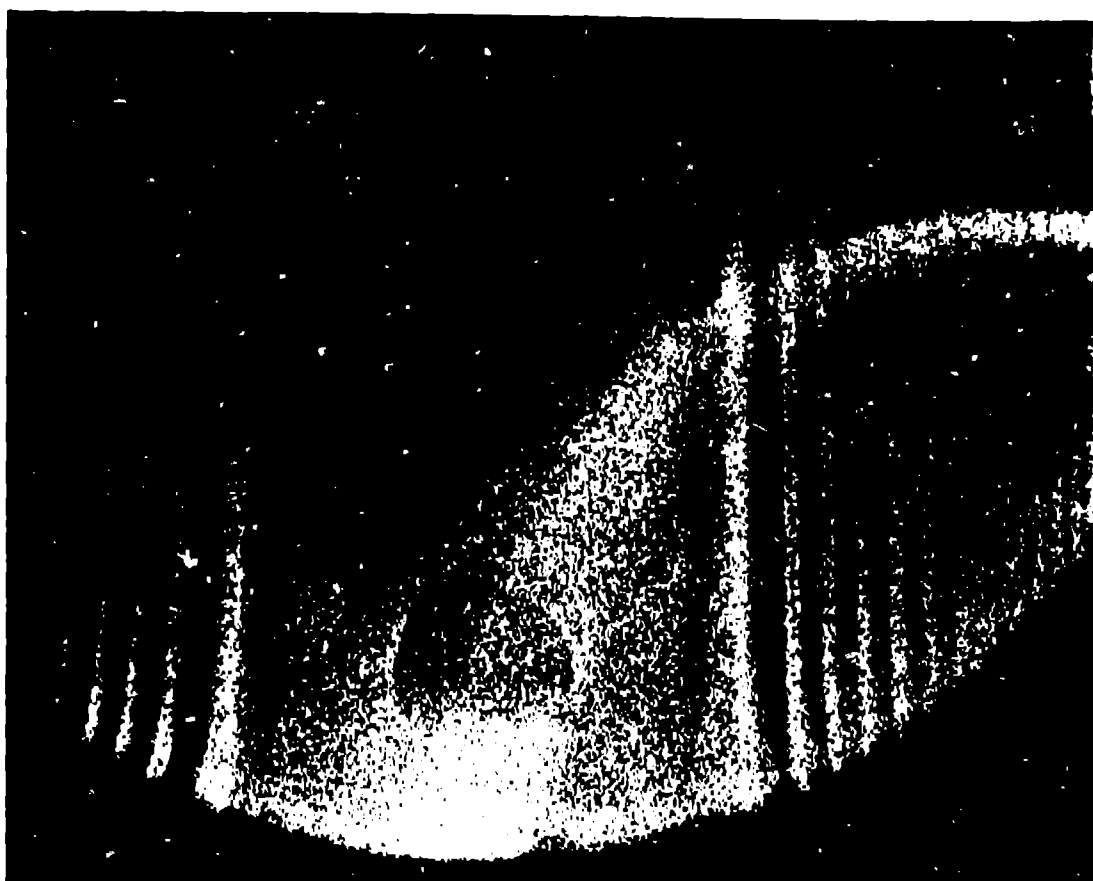


Figure 9: (a) Top view, time integrated pellet trajectory, shot #26921. Launched from the high side port (out of the field of view at the bottom of the picture), along the major radius at 500 m/sec, but deflected strongly to the right. (b) Corresponding density traces. The central density decay time is  $\sim 1$  msec.

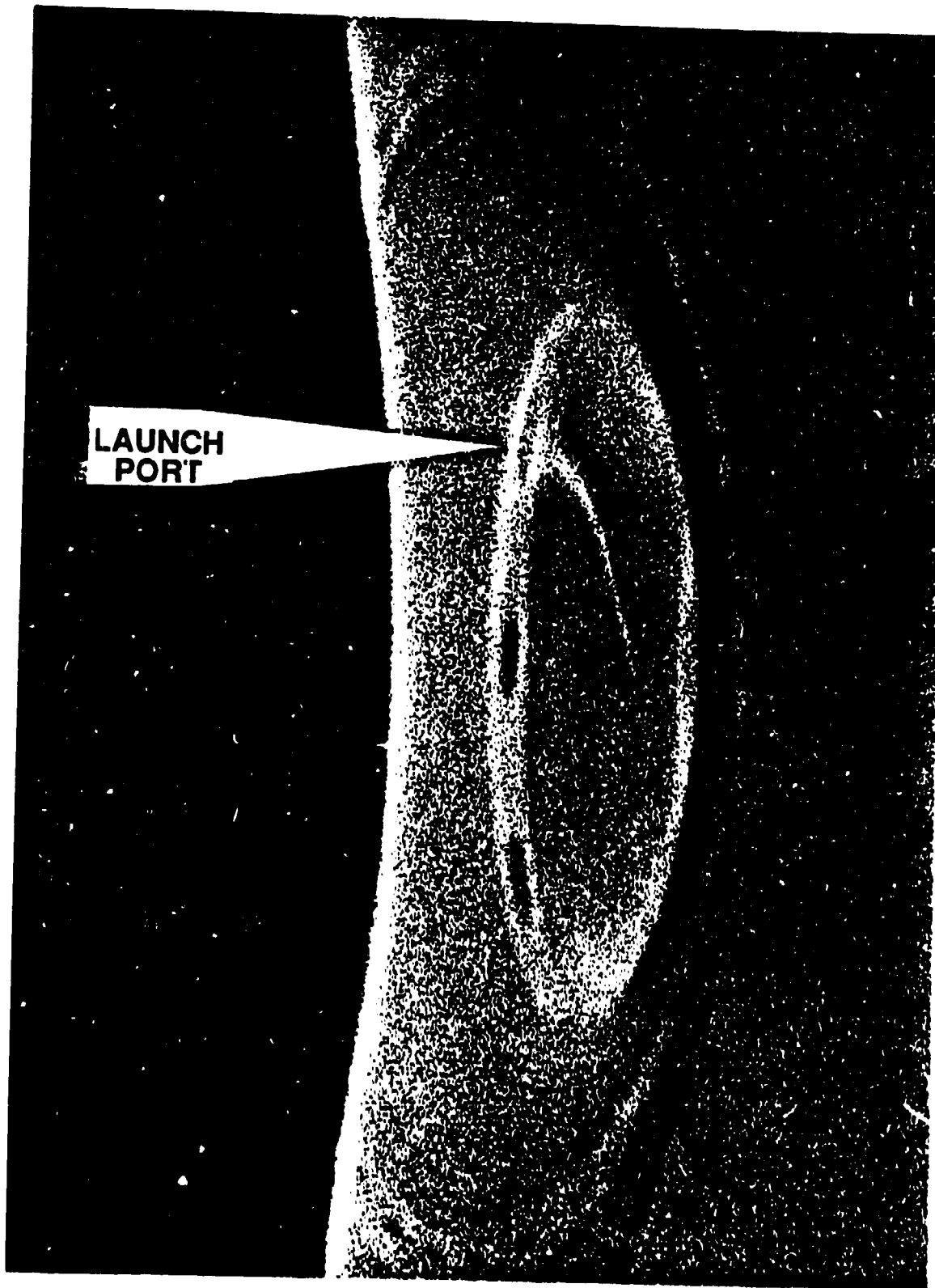


Figure 10: *High side launch time integrated photo of pellet track, showing deflection of the pellet down towards the axis. Spherical mirror causes the D shaped distortion of the circular plasma cross section.*

A gated intensified CCD camera viewing tangentially is used to make in situ pellet cloud intensity, velocity and position measurements, examples being shown in Figure 11. By gating the camera on for  $5\mu\text{sec}$  repetitively every  $100\mu\text{sec}$ , images of the pellet in flight are obtained, and read out immediately with a PC AT frame grabber. The slice of a spherical mirror used to obtain the tangential view results in some distortion, which is correctable using a straight ruler lowered into the torus for calibration purposes. In spite of the deflector plate, the pellets still curve downwards, although when distortion of the spherical viewing mirror is accounted for, the minor axis was missed by only a few centimeters. It is clear from the images that the strong poloidal deflection takes place in the edge. Pictures also show extremely intense  $D_\alpha$  light near the plasma edge, peaking at radii of 17–15 cm, and then falling through the plasma core and inside radius. This is contrary to the time history of typical tracks in tokamaks[14], and indicates a substantial contribution to the pellet ablation must come from a nonthermal population in the RFP. Additionally, pellets which are highly curving are observed to experience a velocity increase of  $\sim 30 - 40\%$  over their initial launch velocity, in substantial agreement with predictions of the rocket ablation model. Pellets launched from the midplane which have "straight" tracks show little speed change.

Often, in the inner and outer edge region, a "comet tail" of  $D_\alpha$  light is seen in the tangential images extending poloidally away from the "electron wind", apparently along field lines. Occasionally, top view pictures show similar tails, but this time in the toroidal projection for the central plasma regions. Both observations are consistent with asymmetric ablation by electrons along magnetic field lines.

### e) Plasma Response to Pellets

With pellet injection, the loop voltage increase is comparable to the toroidal current decrease (usually  $\sim 5\%$ ), but a substantial transient increase in input power to the plasma comes from an expansion of the plasma column (weakening of the field reversal), sometimes as much as doubling the input power. Soon after the pellet is in the plasma edge ( $\delta t \leq 30\mu\text{sec}$  after the initial rise in  $D_\alpha$ ), the central soft x-ray flux begins to fall, and a decrease in the central electron temperature is seen *before* the density rise is observed from the pellet. Momentarily at least, three important variables— $n_e$ ,  $T_e(0)$ , and  $\tau_E$ , are all degraded. Preliminary inferences from a continuum bremsstrahlung "Z-meter"[29] indicate a substantial improvement in  $Z_{eff}$ , however not enough to prevent an increased resistivity. As fueling overcomes a momentary decrease in  $\tau_p$ , the density increases rapidly, and the drop in electron temperature develops further. From the time of maximum density, and during its decay, the  $\beta_e$  is as high or perhaps slightly higher than pre-pellet levels. By 1–2 msec after the pellet density maximum, the plasma recovers pre-pellet electron temperature, density and resistivity levels, but with noticeably lower soft x-ray flux. Vertical and horizontal equilibrium field feedback control systems often respond dramatically, but irreproducibly to the pellets. On the whole, the plasma is remarkably resilient to very large density rises ( $\delta n/n \sim 6$ ), without catastrophic ef-

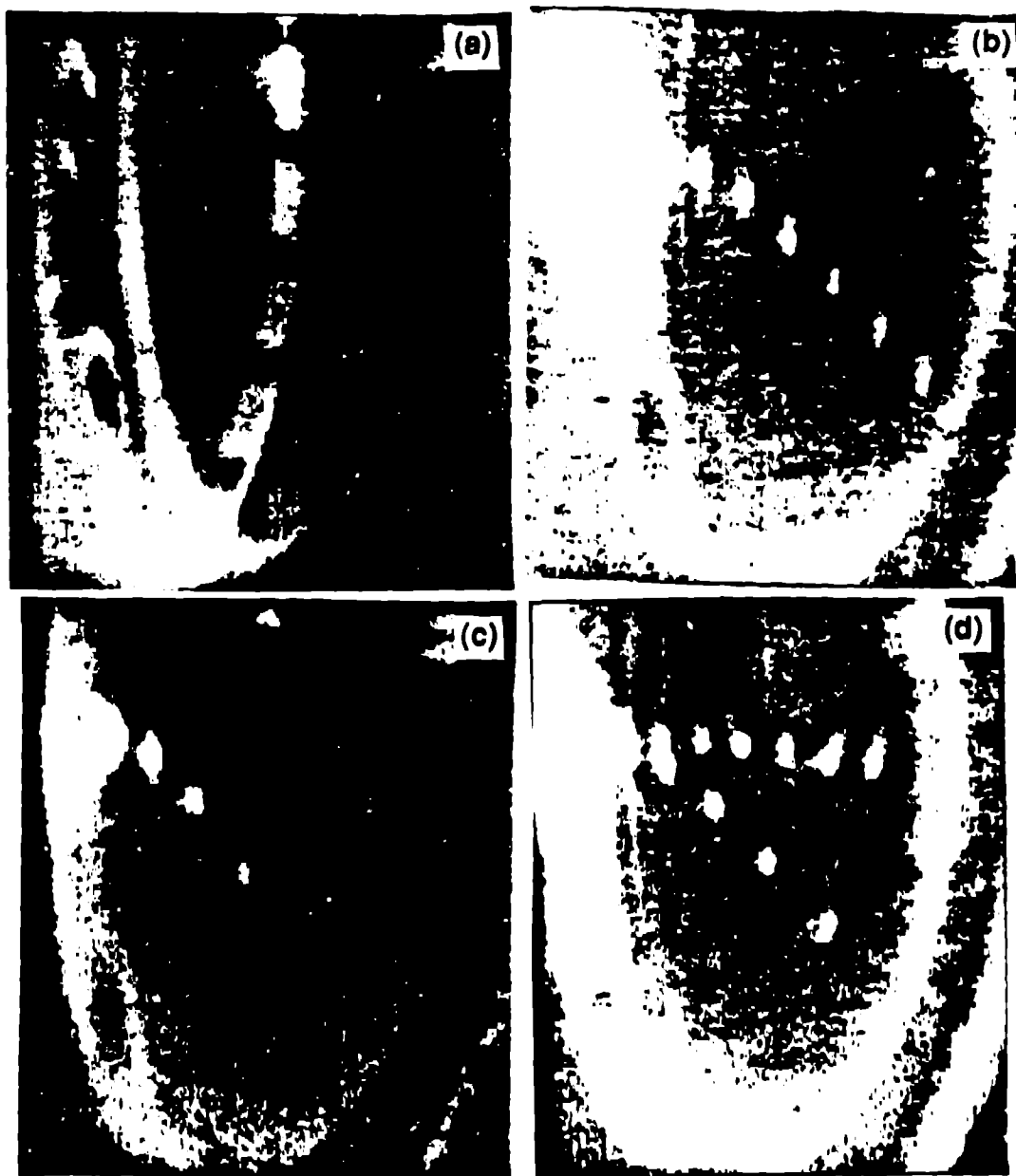


Figure 11: Time resolved tangentially viewing CCD  $D_{\alpha}$  camera images of pellets launched at the midplane with "ski jump". The camera is gated on for 5  $\mu\text{sec}$  every 100  $\mu\text{sec}$ . (a) Calibration image, with 2.8 cm wide, vertical metal ruler in the torus. Dark 'tic' marks, 1.9 cm wide, are spaced every 5 cm. (b) Single deuterium pellet, shot #90106 with upwards launch angle of  $8-16^{\circ}$ , but still deflected downwards, missing the axis by  $\sim 3$  cm. (c) Shot #90112, fully ablated pellet, brightest in the edge. (d) Shot #90111, two pellets, separated in arrival time by 450  $\mu\text{sec}$ . The first to arrive is the more strongly deflected.

fect. Perturbation of the plasma sufficient to cause loss of reversal must be avoided, as the plasma quickly terminates in that situation.

The electron temperature falls nearly linearly in proportion to the line average electron density due to a pellet. A best fit to Thomson scattering data (each point is a single shot) shown in Figure 12(a), predicts that  $T_e(0) \propto \bar{n}_e^{-0.9 \pm 0.1}$ , at the 95% confidence level, for  $I_\phi = 145 \pm 15$  kA.  $\beta_e$  versus  $\bar{n}_e$  shows signs of leveling out at high density. For the same shots, but not necessarily coincident with the

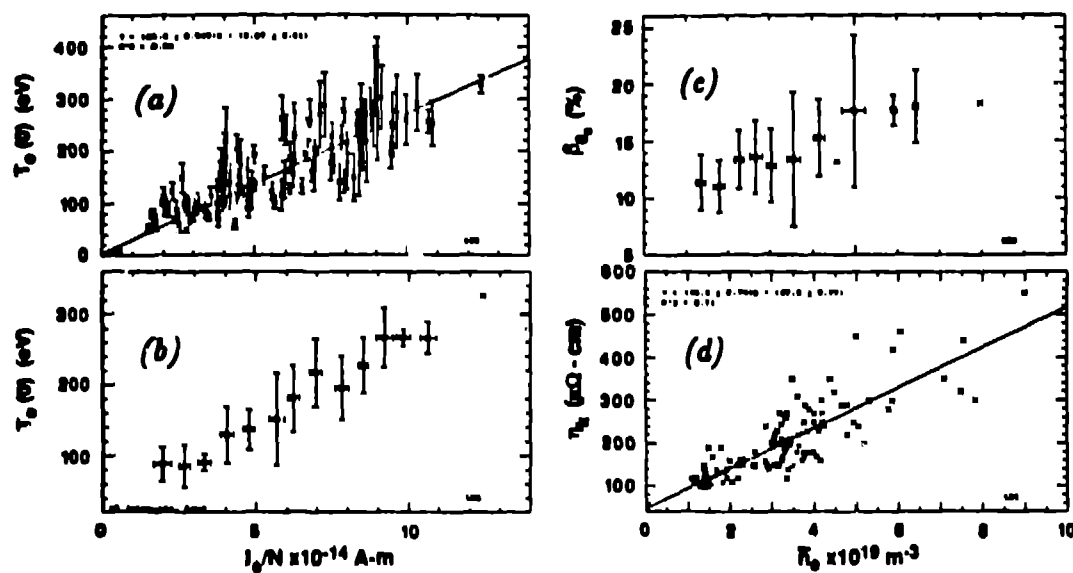


Figure 12:  $T_e$  and  $\eta$  effects during pellet injection for nominal 150 kA discharges. (a)  $T_e(0)$  plotted vs.  $I/N$  for with pellets. (b) Same data as in (a), but averaged into 15 bins. (c)  $\beta_e$  increases weakly with density and may saturate at high density. (d)  $\eta_h$  increases with peak  $\bar{n}_e$  due to pellets.

Thomson time, we can plot the transient rise in helicity based resistivity versus the maximum line average electron density seen on the central FIR interferometer chord (located at least 60 degrees toroidally away from the pellet injection port). A regression on the data yields  $\eta_h \propto \bar{n}_e^{-0.7 \pm 0.1}$ . Assuming classical resistivity scaling, then the two pieces of information together imply that  $Z_{eff} \propto \bar{n}_e^{-0.68 \pm 0.25}$ , assuming similar profiles in all cases.

The ion temperature is monitored by a number of methods, principally Doppler broadening[30] of CV and OVII, but also with time of flight Deuterium charge exchange neutrals, and to a lesser extent neutron emission. Figure 13 shows the ion temperature as measured by the TOF neutral particle spectrometer ( $\blacktriangle$ ), and Carbon V Doppler broadening ( $\bullet$ ). The Thomson scattering central electron temperature at 8 milliseconds is  $T_e(0) = 77 \pm 6$  eV, comparable to the 90 eV ion temperature at that time. The electron density, central SBD x-ray signal, and four  $D_\alpha$  channels in the array, are shown as well. Two pellets entered the plasma, the first one curved strongly and shielded the second one, which penetrated deeply across the column. This is the same shot as shown in the time resolved tangential view photo in Figure 11(d). Before the pellet arrives,  $T_i \simeq 200 - 250$  eV. It quickly falls to  $\sim 90 - 100$  eV, and then recovers in 1-2 msec to near 200 eV again. Crudely,

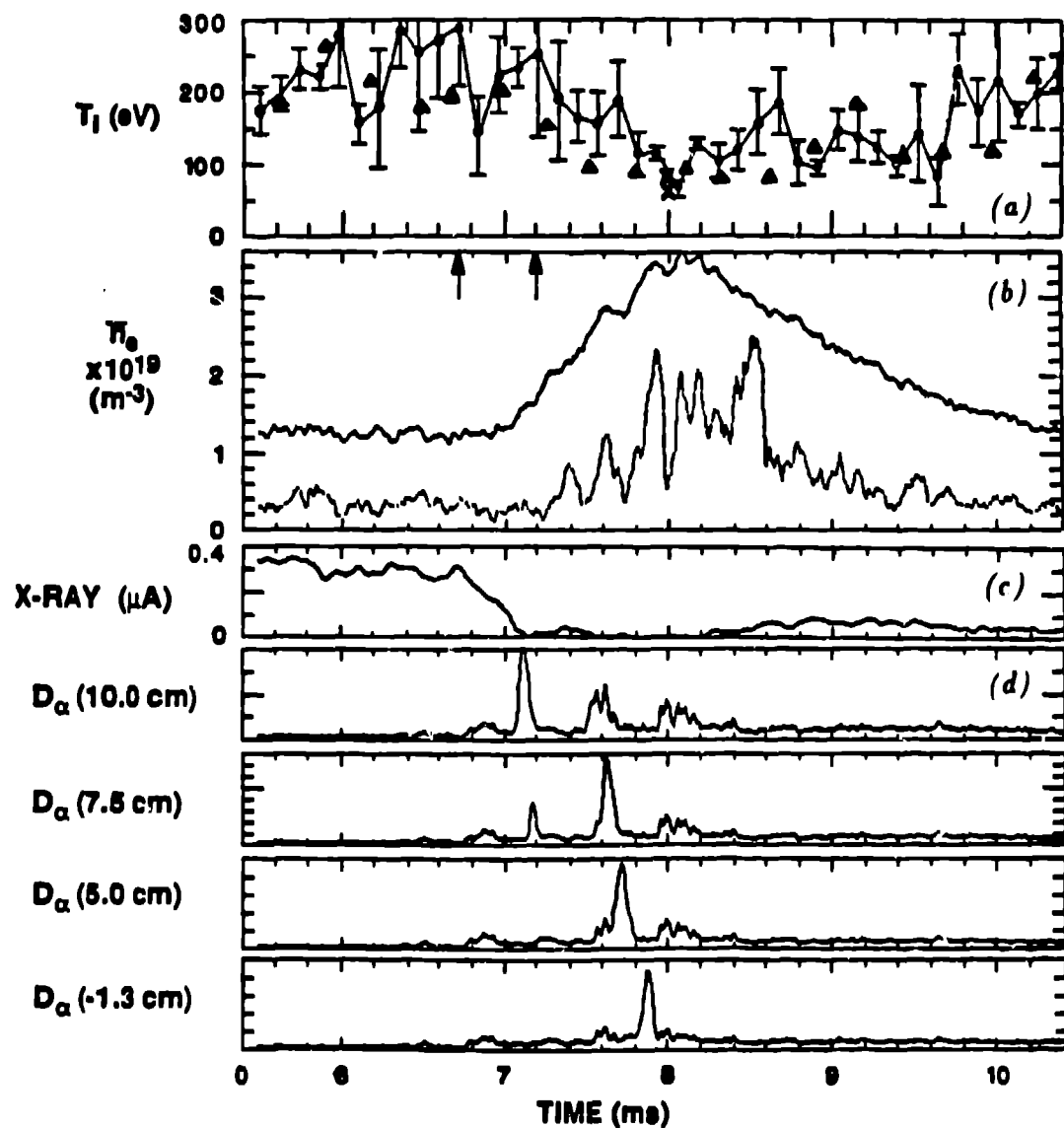


Figure 13: *Response to a pellet. (a) Ion temperature measured by TOF deuterium neutrals ( $\blacktriangle$ ), by CV Doppler broadening ( $\bullet$ ), and one point of  $T_e(0)$  by Thomson scattering ( $\circ$ ). (b) Electron density along +4 cm and +16 cm chords. (c) Soft x-ray SBD center chord. (d) Pellets seen on the  $D_\alpha$  array chords, from 10, 7.5, 5.0, and -1.3 cm lines of sight at the plasma midplane.*

it appears that a limit in poloidal beta is controlling the physics. Interestingly, the TOF system shows there are radical changes taking place globally in the deuterium recycling flux as a result of the pellet. Near the time of peak density, the TOF actually has a difficult time getting signals, due to a large drop in neutral emission at its toroidal location.

For 100→200 kA ramped discharges, where OVII line broadening, neutron rate, and CV Doppler can be used, the ions have too high a temperature to be measured with the TOF system (ie.,  $T_i > 500\text{eV}$ ). Neutron emission may have a short burst due to the pellet, but then the rate drops and it does not recover to detectable levels during the remainder of the discharge. CV Doppler, which has sufficient photon flux for single shot measurements, shows a rapid fall from 500–600 eV (for  $\Delta n_e = 3.9 \times 10^{19}\text{m}^{-3}$ ) to 150 eV, but then only recovers to the 200–300 eV level. However, its spatial position in the plasma column for peak emission is known to be moving, hence core temperature inferences are dangerous. A further complication involves possible changes in charge exchange losses, which may remain at enhanced levels after a pellet event. Clearly, further measurements are required to understand the mechanisms and implications. This actually applies to all parameters lacking in radial or temporal resolution.

## V. Summary

We have seen that control of density can be achieved through a combination of wall conditioning, gas puffing and pellet injection. In the future, divertors may also play a role in RFPs in this endeavor. However, the next generation RFPs face the immediate problem of dealing with the large surface area of 100% graphite armor walls, in addition to reduced neutral gas penetration depths as  $T_e$ ,  $\bar{n}_e$ , and minor radius all get larger.

On timescales of 1 second, the wall recycling can be expected to be even more critical than in the present pulse length machines. Feedback controlled gas puffing will be as commonplace as it is in tokamaks. However, due to higher  $\bar{n}_e$  (expected to be  $\sim 2 - 8 \times 10^{21}\text{m}^{-3}$ ) in ZTH and RFX, problems with edge refueling are likely. Pellet injection at speeds of 1–1.5 km/sec is technologically at hand, and appears adequate to do the job. As the particle confinement time lengthens at higher currents, pellets can be launched less frequently. A range of sizes in the pellets from  $r_{\text{pel}} \approx 0.5 - 2\text{ mm}$  is needed both for purposes of variable penetration, and stacking if desired. The electron drift parameter is expected to be lower in the larger machines, so that poloidal deflection of pellets is less likely to be a problem, although provisions for side launch 10–15 cm above the axis are being made for ZTH. In the interim, pellets offer an approach to a cleaner plasma, and provide a unique transient diagnostic probe of many plasma parameters, including possibly information about the RFP reversal layer.

## Acknowledgments

We would like to thank the ZT-40M operations and diagnostics teams, Dr. M.

Greenwald at MIT for the core of the Alcator C pellet injector, and ORNL pellet group (especially Dr. D. Schuresko) for their support. This work is supported by the U. S. Dept. of Energy.

## References

- [1] BUFFA, A., COSTA, S., DeANGELIS, R., GIUDICOTTI, L., GOWERS, C. W., et al., in *Plasma Physics and Controlled Nuclear Fusion Research, 1980* (IAEA, Vienna, 1981) p. 275, Volume II (Brussels Conference), 1980.
- [2] BAKER, D. A., BAUSMAN, M. D., BUCHENAUER, C. J., BURKHARDT, L. C., CHANDLER, G. et al., in *Plasma Physics and Controlled Nuclear Fusion Research, 1982* (IAEA, Vienna, 1983) p. 587, Volume I (Baltimore Conference), 1982.
- [3] TAMANO, T., CARLSTROM, T., CHU, C., GOFORTH, R., JACKSON, G., et al., in *Plasma Physics and Controlled Nuclear Fusion Research, 1982* (IAEA, Vienna, 1983) p. 609, Volume I (Baltimore Conference), 1982.
- [4] MASSEY, R. S., WATT, R. G., WEBER, P. G., WURDEN, G. A., BAKER, D. A., et al., *Fusion Technology* **8** (1985) 1571.
- [5] NEWTON, A. A., JARBOE, T., FIRTH, L., and NOONAN, P. G., *Journal of Nuclear Materials* **145-147** (1987) 487.
- [6] POST, D. E. and BEHRISCH, P., editors, *Physics of Plasma-Wall interactions in Controlled Fusion* (Plenum Press, New York, 1984), NATO Advanced Science Institutes Series, Series B Vol. 131.
- [7] JACKSON, G. L., TAYLOR, T. S., CARLSTROM, T. N., CURWEN, B., GOFORTH, R. R., et al., *Journal of Nuclear Materials* **145-147** (1987) 470.
- [8] CAYTON, T. E., DOWNING, J. N., WEBER, P. G., BAKER, D. A., BASTASZ, R. J., et al., *Journal of Nuclear Materials* **145-147** (1987) 71.
- [9] JACOBSON, A. R. and RUSBRIDGE, M. G., Technical Report LA-9589-MS, Los Alamos National Laboratory (1982).
- [10] WURDEN, G. A., WELDON, D. M., WEBER, P. G., WATT, R. G., SCHOFIELD, A. E., et al., *Bulletin of the American Physical Society* **30** (1985) 1402 [San Diego, Nov. 1985, DPP Meeting].
- [11] ALPER, B., EVANS, D. E., STOREY, D. P., and TSUI, H., *Bulletin of the American Physical Society* **30** (1985) 1406 [San Diego, Nov. 1985, DPP Meeting].
- [12] ALPER, B., MARTINI, S., and ORTOLANI, S., *Nucl. Fusion* **20** (1986) 1256.

- [13] See Proceedings of this School, G. A. Wurden.
- [14] MILORA, S. L., *Journal of Fusion Energy* **1** (1981) 15.
- [15] WURDEN, G. A., *Bulletin of the American Physical Society* **31** (1986) 1412 [Invited Talk, Baltimore, Nov. 3-7, 1986, DPP Meeting].
- [16] WURDEN, G. A., WEBER, P. G., WATT, R. G., MUNSON, C. P., INGRAHAM, J. C., et al., *Nucl. Fusion* **27** (1987) 857.
- [17] ANTONI, V., BUFFA, A., CARRARO, L., COSTA, S., SIMONE, P. D., et al., in *Plasma Physics and Controlled Nuclear Fusion Research, 1986* (IAEA, Vienna, 1987) p. [Volume I (Kyoto Conference), 1986].
- [18] GREENWALD, M., GWINN, D., MILORA, S., PARKER, J., PARKER, R., et al., *Phys. Rev. Lett.* **53** (1984) 352.
- [19] WATT, R. G., WURDEN, G. A., WEBER, P. G., BÜCHL, K., and SPANOS, E. K., *Rev. Sci. Instr.* (1987) [Accepted for publication].
- [20] WEBER, P. G., in *International School of Plasma Physics, Course on Plasma Diagnostics* (Varenna, Italy, 1986).
- [21] PARKS, P. B., TURNBULL, R. J., and FOSTER, C. A., *Nucl. Fusion* **17** (1977) 539.
- [22] MILORA, S. L. and FOSTER, C. A., *IEEE Trans. Plasma Sci.* **PS-6** (1978) 578.
- [23] HOULBERG, W. A., MILORA, S. L., and ATTENBERGER, S. E., *Neutral and Plasma Shielding Model for Pellet Ablation*, 1987, to be published.
- [24] OGAWA, K., MAEJIMA, Y., SHIMADA, T., HIRANO, Y., and YAGI, Y., *Nucl. Fusion* **25** (1985) 1295.
- [25] NEWTON, A. A., in *International Workshop on Engineering Design of Next Step RFP Devices* (Los Alamos National Laboratory, 1987) [July 13-17, 1987].
- [26] WATT, R. G. and LITTLE, E. M., *Phys. Fluids* **27** (1984) 784.
- [27] SCHOENBERG, K. F., INGRAHAM, J. C., ELLIS, R., WEBER, P. G., DOWNING, J. N., et al., in *14<sup>th</sup> European Conference on Controlled Fusion and Plasma Physics* (European Physical Society, Madrid, 1987) p. [LA-UR-87-1616].
- [28] JONES, R., *Plasma Phys.* **22** (1986) 813.
- [29] WEBER, P. G., *Phys. Fluids* **28** (1985) 3136.
- [30] HOWELL, R. B. and NAGAYAMA, Y., *Phys. Fluids* **28** (1985) 743.

## **DISCLAIMER**

This report was prepared as an account of work sponsored by an agency of the United States Government. Neither the United States Government nor any agency thereof, nor any of their employees, makes any warranty, express or implied, or assumes any legal liability or responsibility for the accuracy, completeness, or usefulness of any information, apparatus, product, or process disclosed, or represents that its use would not infringe privately owned rights. Reference herein to any specific commercial product, process, or service by trade name, trademark, manufacturer, or otherwise does not necessarily constitute or imply its endorsement, recommendation, or favoring by the United States Government or any agency thereof. The views and opinions of authors expressed herein do not necessarily state or reflect those of the United States Government or any agency thereof.